AN ABSTRACT OF THE THESIS OF

Ye Liu for the degree of Master of Science in Electrical and Computer Engineering presented on November 22, 2016.

Title: Quantum Dots-Fullerene Based Molecular Beacons for Highly Sensitive DNA Detection.

Abstract approved: _____

Li-Jing Cheng

We demonstrated a low-cost and high-sensitivity DNA detection method using quantum dot-fullerene based molecular beacons (MBs) and magnetic nanoparticles. The MB tethered magnetic nanoparticles can be well dispersed in analytes for efficient DNA capture and concentrated by an external magnetic field for enhanced fluorescence signal detection. The detection requires only 5 μl analyte samples and takes about 20 minutes. The high signal-to-noise ratio produced by the quantum dot-fullerene pairs and magnetic concentration yield a detection limit as low as 100 fM.

Quantum Dots-Fullerene Based Molecular Beacons for Highly Sensitive DNA Detection

by

Ye Liu

A THESIS

submitted to

Oregon State University

in partial fulfillment of
the requirements for the
degree of

Master of Science

Presented November 22, 2016
Commencement June 2017

Master of Science thesis of Ye Liu presented on November 22, 2016

APPROVED:

Major Professor, representing Electrical and Computer Engineering

Director of the School of Electrical Engineering and Computer Science

Dean of the Graduate School

I understand that my thesis will become part of the permanent collection of Oregon State University libraries. My signature below authorizes release of my thesis to any reader upon request.

Ye Liu, Author

ACKNOWLEDGEMENTS

I would like to express deepest gratitude to my advisor Dr. Larry Cheng for his full support, expert guidance, understanding and encouragement throughout my study and research. In addition, I express my appreciation to Dr. Alan Wang, Dr. Matthew Johnston, Dr. Alex Chang , and Dr. Jimmy,Yang for having served on my committee. Their thoughtful questions and comments were valued greatly.

I would also like to thank instructors for helping me with my coursework and academic research during my graduate years at Oregon State University.

Thank you to everyone in the Larry Group (past and present) for your assistance and sharing space. Akash, Bo, and Vishvas.

Thank you to all of my friends in OSU. You are all great. Zheng Zhou, Guo Hengma, ZiJie Zhu, Yue Liu, YongBin Gu, YunFan Li, XinYuan Zhong, I will remember all the fun memories and late-night study sessions we had together.

Finally, I would like to thank my wife and my parents for their unconditional love and support during the last two years; I would not have been able to complete this thesis without their continuous love and encouragement.

TABLE OF CONTENTS

Page

LIST OF FIGURES

LIST OF FIGURES (Continued)

Figure Page

1. Introduction

1.1 DNA and DNA detection technologies

Deoxyribonucleic acid (DNA) is a linear polymer composed of a backbone where phosphates alternate with deoxyribose sugar and a nucleotide base is attached to each sugar. Four nucleotide bases of a DNA strand — adenine (A), cytosine (C), guanine (G), thymine (T) — covalently linked to the deoxyribose sugar. Hybridization of two single-stranded DNA with complementary sequences constructs a double-stranded DNA. The hybridization takes place through the hydrogen bonding between base A and base T or base C and base G. The base pairs can dissociate or denature at low ionic strength, high pH condition or high temperature. The DNA of each species contains unique fingerprint sequences. We can recognize the specific types of pathogens by detecting their specific sequences through the hybridization of the target DNA with a probe with a complementary sequence. The capture of target DNA will later be transduced into measurable signals, such as optical emission or electrical readouts.

Traditional DNA detection techniques utilize polymerase chain reaction (PCR) to amplify DNA number and mark the DNA copies with radiolabels so that they can be quantified under radiation. In spite of its high detection sensitivity, the radioactive detection is dangerous, expensive and time-consuming—typically a one-day long assay [5]. Other technologies measure DNA through optical illumination and photodetection. Lia et al. immobilized DNA probes on a photodiode to detect target DNA by measuring the reduction of transmissive light due to the light scattering from gold nanoparticles in response to the number of the captured target DNA [6]. The detection signal is

amplified when the gold nanoparticles are enlarged by a further coating of silver. The technique reaches a detection limit of 10 pM. DNA detection can also be performed by using electrochemical redox reaction on a microelectrode [7].

Surface plasmon resonance (SPR) has been demonstrated to offer good stability and sensitivity in nucleic acid detection. Misono et al.[8] reported the binding of hemagglutinin to an SPR device for RNA capture. The RNA enrichment improved the detection sensitivity.

Artificial nucleic acid has been widely used to improve the sensitivity and selectivity of DNA detection, such as locked nucleic acid (LNA), peptide nucleic acid (PNA), and hexitol nucleic acid (HNA). Zheng et al.[9] used LNA molecular beacons for DNA detection. The molecular beacon composed of 6-FAM and DABCYL as the fluorophore and quencher, respectively, achieved a detection limit of 11 nM unassociated with PCR technology.

Fluorescence-based signal detection is one of the most sensitive and accurate approaches for DNA detection. However, most of the detection requires additional labeling steps in the assay to attach fluorescence tags to the hybridized DNA. The process can be simplified by using molecular beacons (MBs) with prelabelled fluorescence tags. A typical MB structure illustrated in Fig. 1.1, consists of a fluorophore and a quencher immobilized in the two ends of a DNA probe. Such DNA probe is designed to have a sequence that tends to self-hybridize a hairpin structure with a loop containing a sequence complementary to the target DNA and a stem paired by the short segments of sequence located at the two ends of the probe. The MB stays in the hairpin structure in the absence of target and has the quencher in the vicinity to the fluorophore resulting in the fluorescence quenching. In the present of target DNA, it hybridizes with the loop segment and

denatures the stem segment. As a result, the fluorophore leaves the quencher and emits light under excitation. Also, the fluorescence of MBs can restore at a temperature higher the melting temperature of the hybridized stem because the dissociation of stem separates the quencher-fluorophore pairs at such high temperature.

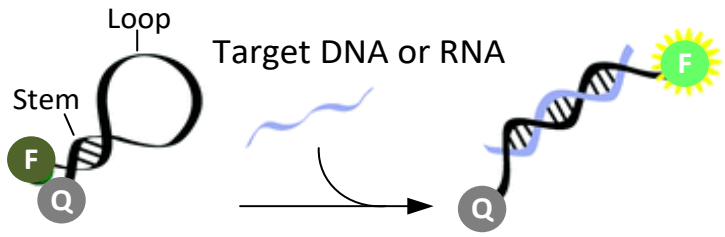

Figure 1.1 Structure of a DNA molecular beacon (MB).

1.2 Fluorophores and Quantum Dots

Different kinds of fluorophores have been applied in biosensors and biomedical fields, such as organic fluorophores, metal nanoclusters, carbon dots, dye-doped nanoparticles, lanthanide-doped matrix and quantum dots (QDs). Among them, QDs and organic fluorescence dyes are sufficiently small to serve as the fluorophore for a DNA-MB. QDs are nano-sized semiconductor crystals that emit light when excited by a radiation of sufficient energy. The electrons in QDs are confined in a space smaller than the exciton Bohr radius, resulting in quantization of the energy levels. As the size of the QDs decreases, the difference in energy between the highest valence band and the lowest conduction band increases as shown in Fig. 1.2. The size of QDs determines their optical properties. A small-sized crystalline nanoparticle is accompanied by a large band gap, so the optical absorption and emission can blue shift in wavelength comparing with a large-sized

counterpart. Compared with traditional organic dyes, QDs are superior in their broad absorption and narrow emission, high photostability, and high chemical stability, which are very suitable for a variety of applications. Quantum dot emission is adjustable by tuning its size. Under the same excitation, QDs with different sizes can emit different colors. This offers feasibility of multi-target detection.

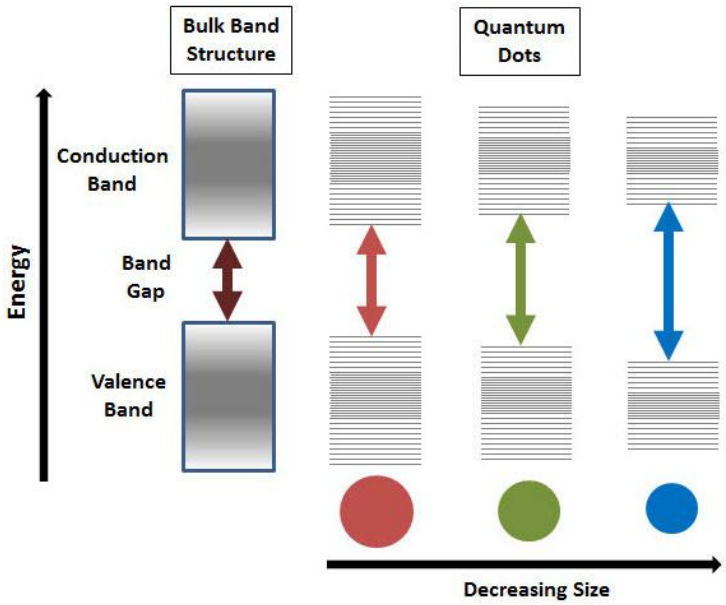

Figure 1.2 Band diagrams of block and nanocrystal semiconductor with various particle sizes.

The surface of nanocrystal particle is not stable in nanoscale. The surface area-to-volume ratio increases with the decrease of particle size, leading to an increased surface energy. The repellent forces among atoms make an unstable surface, which leads QDs more reactive; for instance, it can be oxidized easily. The energetic atoms are reactive and will cause lattice deformation, thus affect the optical properties. To maintain a stable optical property, the QDs can be coated with a layer of semiconductor materials, such as ZnS, with a similar lattice constant to that of the core. The QDs surface can also be stabilized by organic surface ligands [10].

1.3 C_{60} fullerene quencher for quantum dots

Fullerene can be used to quench a quantum dot. Fullerene (C_{60}) is a carbon-based material in the form of a soccer structure. C_{60} contains twelve pentagonal rings and twenty hexagonal rings with a diameter of 0.8 nm in average [1]. The carbon atoms within C_{60} are sp^2 and sp^3 hybridized. C_{60} has a unique thermostability and low toxicity. Recently, the charge transfer properties of C_{60} has been widely studied and has been proven to have a large potential to advance the performance of light-emitting diode, solar cell, and biosensor.

When conjoint C_{60} on a quantum dot surface, the quantum dot luminescence can be efficiently quenched. The quenched QDs express long "off" state in dynamic trajectories of PL intensity and shorter lifetime [2]. C_{60} has its lowest unoccupied molecular orbital (LUMO) at -4.7 eV, and highest occupied molecular orbital (HOMO) at -6.8 eV [3]. As shown in Fig. 1.3, when a C_{60} is placed in the vicinity to a CdSe quantum dot, it tends to uptake the excited electron in the CdSe quantum dot and quenches emission through electron transfer. In an excited C_{60} conjoined quantum dot (C_{60}-QD), the large population of electrons in the quantum dot will transfer to the acceptor C_{60} instead of recombining with a hole on valence band; as a result, the C_{60}-QD complex emits fewer photons. Electron transfer rate is higher for a smaller sized QDs conjoined by C_{60} because there is a larger potential energy drop between the conduction band and LUMO [15].

Another QDs quenching mechanism using C_{60} is through Förster resonance energy transfer (FRET). Michael H. et al. addressed that the spectral overlap between QDs emission and C_{60} absorption spectrum results in different quenching efficiency along quantum dot emission

wavelengths [4]. High energy emission QDs, such as the QDs with 450nm emission wavelength, are likely to be quenched through FRET because the C_{60} has stronger absorption at a shorter wavelength.

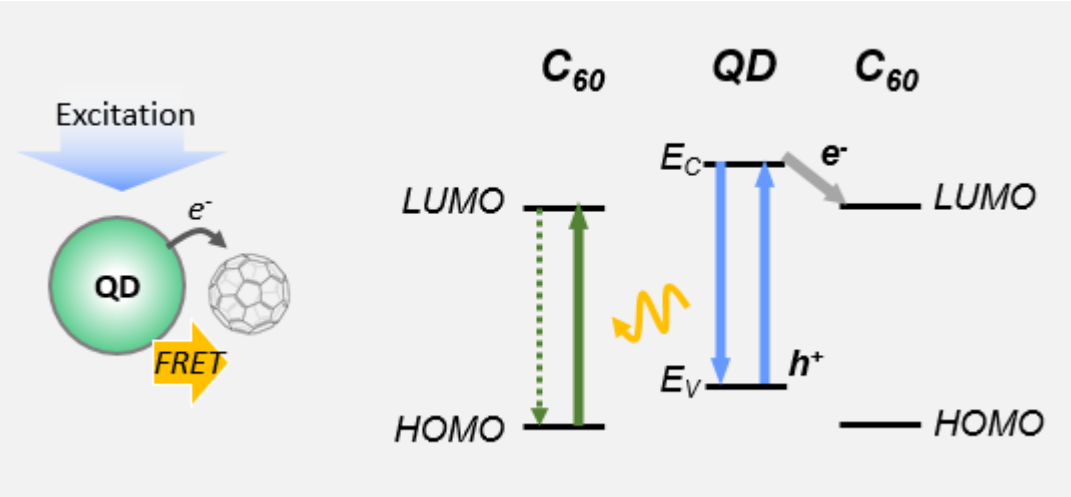

Figure 1.3. Schematic represents C_{60} quenches a QD through two pathways: electron transfer (ET) and Förster resonance energy transfer (FRET) [4].

1.4 Energy transfer and quenchers

There are several molecules available for quenching organic dyes, but it is hard to find a proper material to quench QDs. It is suggested that QDs are typically quenched through fluorescence resonance energy transfer (FRET) and charge transfer. FRET is a preferred process when QDs emission wavelength matches the absorption peak of the quencher. The energy from a quantum dot can be transferred to a quencher nearby, preventing quantum dot from emission.

Nathaniel et al.[11] compared the quenching efficiency of Iowa Black, 1.4 nm-sized gold nanoparticle, and Dabcyl molecule for quenching 525 nm QDs MB. A quenching efficiency of about 70% was observed by using Iowa Black and gold nanoparticles. Dabcyl molecule's

absorption does not overlap with the emission of 525 nm QDs which shows only 50% quenching efficiency, while Iowa Black does gives a 80% quenching efficiency. The gold nanoparticle is an efficient quencher for QDs, but the experimental quenching efficiency varies with different QDs emission and experimental conditions. Zoher et al.[12] reported the 1.4 nm diameter gold can quench the 522 nm QDs up to 83% at an interparticle distance of 5.9 nm with a 1:1 quencher-QD ratio. The quenching efficiency reaches almost 100% at an interparticle distance of 4 nm and decreases as the distance increases. Hsiao et al.[13] used gold nanoparticles to quench 550 nm emission QDs and achieved 37% quenching efficiency in 1:1 quencher-QD ratio and 91% quenching efficiency in 6:1 ratio.

As a small-sized quencher, C_{60} offers a comparable quenching performance to a 1.4 nm-sized gold nanoparticle. However, C_{60} was found to quench quantum dot emission mostly through electron transfer. Nianhu, Kirsi Virkki et al.[14, 15] proved that the electron-transfer rate increases with the C_{60}-to-QD ratio. Zhihua et al.[16] demonstrated that the quenching efficiency strongly depends on the distance between quantum dot and C_{60}.

QDs size determines how efficient a C_{60} can quench it. C_{60} quenches small-sized QDs more efficiently because the higher conduction band in the small QDs results in a large potential difference relative to the LUMO of C_{60} and thus increases the electron transfer rate[10]. C_{60} can serve as a good quencher for QDs. Kirsi et al.[15] reported an 80% quenching efficiency for the QDs with 540 nm and 630 nm emissions, and above 90% for the QDs with 570 nm and 600 nm emissions with 2:1 C_{60}-to-QD molar ratio.

Michael H. et al.[4] also explained proved that FRET also involves in the process involves in the quenching behavior mechanism in C60-QD pairs. The increased number of C_{60} attached on each QD increases the absorption strength of C_{60} and therefore proportionally increases the FRET efficiency. In their experiments, a 3.3 nm-long peptide linker was used to link C_{60} to a quantum dot. Under a 70:1 C_{60}-to-QD mole ratio, quenching efficiencies of 56%, 77%, and 57% were observed in quenching QDs with 530 nm, 580 nm, and 630 nm emission, respectively.

1.5 Strategy of DNA detection

Many strategies have been developed for optical-based DNA detection. The readout of DNA detection can be achieved by measuring the change in fluorescence intensity or wavelength resulting from the energy transfer from QDs donors to acceptors or quenchers. To amplify the detection signals, the strategy associated with reporter probe and capture probe has been developed. The hybridization detected by conjugating probe DNA onto QDs and monitoring the energy transfer upon hybridization with dye-labeled target DNA [17]. The strategy yields a detection limit of 1 pM. In order to control the effective energy transfer distance, Zhang et al.[18] add an additional capture probe to assist reporter probe for DNA capturing. The captured DNA with probes formed sandwiched hybrid structure, and the structure can attached on the QDs. In a designed distance between QDs and Cy5, the energy can effective transfer (Fig. 1.4).

The DNA sensor based on hairpin MB probes supports label-free detection. The hairpin probes are highly thermodynamically stable and exhibit higher rates of hybridization capture ability than linear probes [19]. Shiping et al.[20] designed a multiple probe nano-sensor by assembling different

fluorophore-labelled hairpin probes on 15 nm gold nanoparticles to detect multiple targets (Fig. 1.5). The limit of detection was 500 pM and the assay time was less than 10 min.

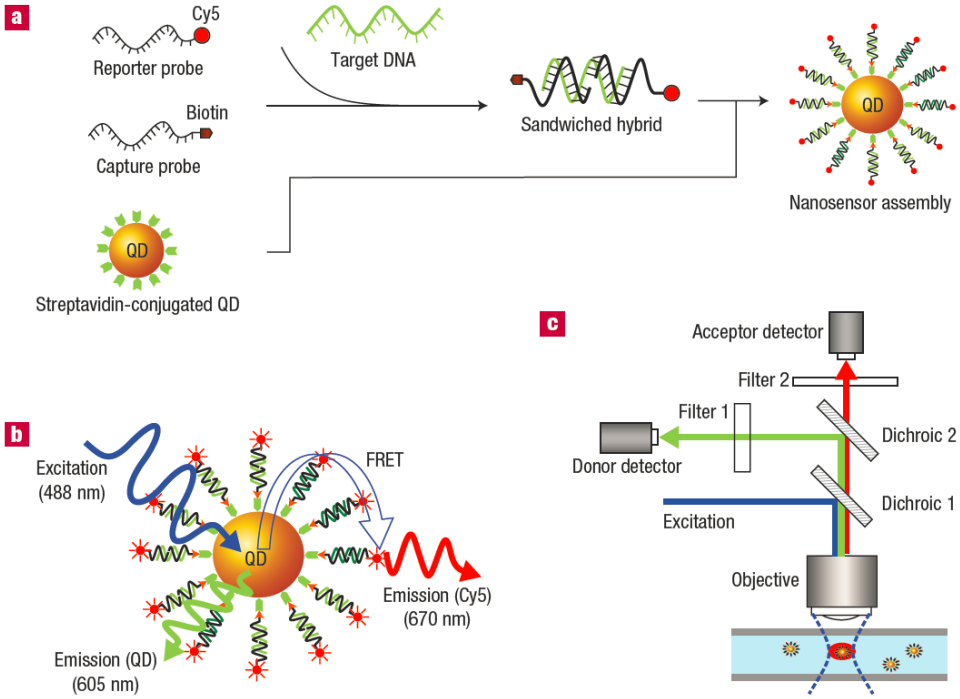

Figure 1.4 Single Schematic of single-QD-based DNA nanosensors. (a) Conceptual scheme illustrates the formation of a nanosensor assembly in the presence of targets. (b) Fluorescence emission from Cy5 on the illumination of the QD caused by FRET between Cy5 acceptors and a QD donor in a nanosensor assembly. (c) Optical setup for fluorescence detection [18].

Each MB-conjugated quantum dot typically contains more than one DNA-MB probe. Hsiao et al.[13] demonstrated DNA sensors based on QD-gold nanoparticle conjugated MBs. The design used 1.4 nm gold as the quencher for QDs. Upon detection, the QDs fluorescence intensity was measured to be 7.3 times brighter than the initial status.

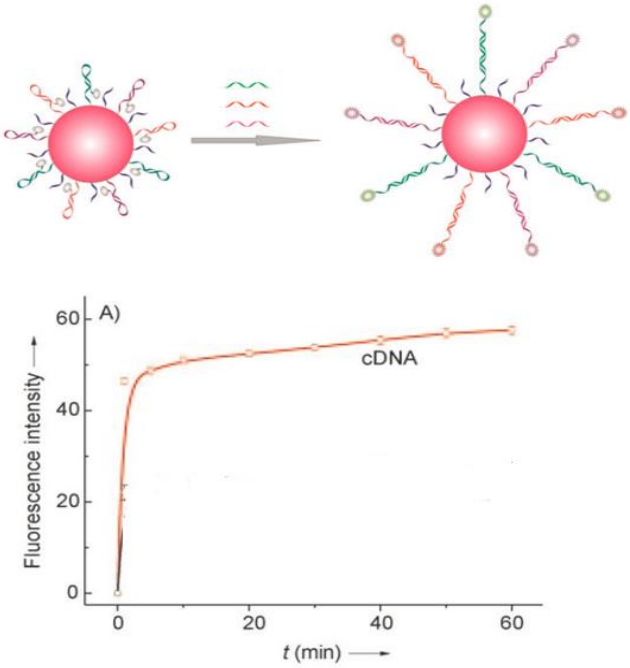

Figure 1.5 Multiprobe nanosensor for multiple DNA detection. The hybridization takes 10 minutes [20].

Nusret Ertas et al.[21] reported DNA detection using probe immobilized QDs for DNA capture and Idarubicin quencher to report the hybridization process. An additional labeling step was carried out to attach Idarubicin to the hybridized double-stranded DNA via π- π interaction, and quenches the quantum dot emission. The detection limit was measured to be 1.2 μM. A similar DNA detection assay was reported by Sara Raichlin et al.[22] who used molecular quencher doxorubicin was used to report the binding of target DNA to the probe immobilized on a quantum dot. The doxorubicin attached to the hybridized duplex structure and quenches QDs by electron transfer. The detection limit reached 10 nM. Doxorubicin supported a 50% quenching efficiency which is not sufficient to achieve a decent detection limit.

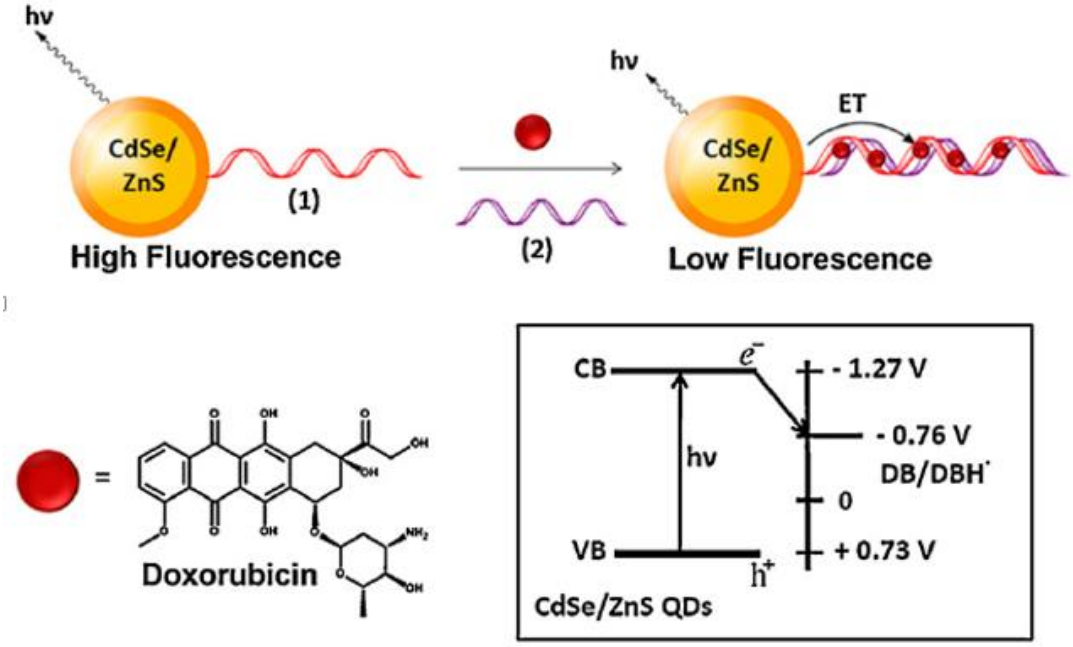

Figure 1.6 A) Detection of DNA by nucleic acid functionalized QDs and doxorubicin, as a quencher. Inset: Energy level diagram corresponding to the electron transfer quenching of the CdSe/ZnS QDs by DB [22].

Most of the carbon-based quenchers are designed to initially bond to fluorophore-labeled DNA probes through π-π interaction. Hybridization of target DNA perturbs the π-π interaction and releases the fluorophore-labeled probes from the carbon-based quenchers [23, 24]. Ronghua et al. reported the use of carbon nanotubes for such type of assay [25]. Fig. 1.7 shows a typical DNA detection assay based on quenching of QDs through π-π interaction between single-stranded DNA probes and graphene oxide (GO).

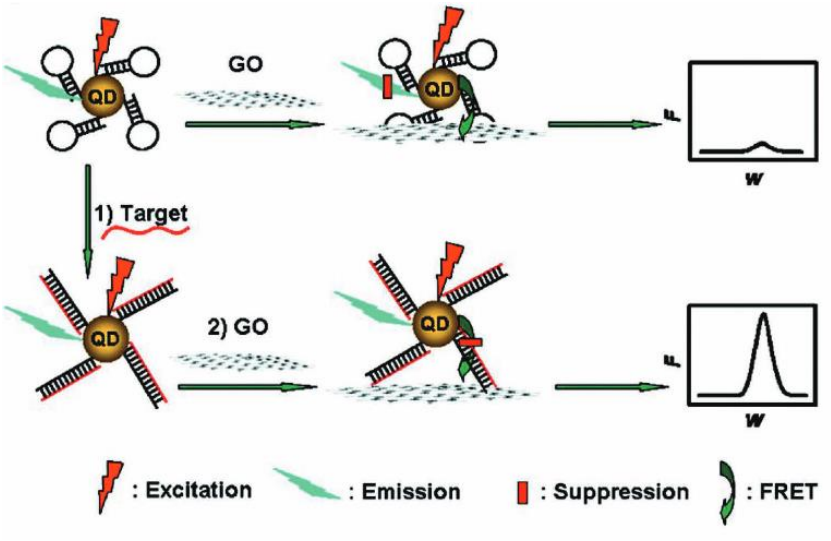

Figure 1.7 Sketch of GO as an acceptor for QDs FRET donors. A) DNA detection. Molecular beacon decorated QDs are quenched onto the GO surface. They detach in response to the hybridization of target DNA resulting in, recovering the QDs emission [26].

1.6 Inspiration and Research Goal

Using hairpin MB probes for nucleic acid detection is advantageous in its high sensitivity and a simplified assay that gets rid of the additional labeling step. Several carbon-based materials can serve as the quencher for QDs, but they have relatively large volume. The large steric effect could deteriorate the capture efficiency of target DNA. The small-sized C_{60} (<1 nm) is suitable for forming a QD-hairpin probe configuration. To our knowledge, the use of C_{60} as the quencher for QD-based MBs has not been reported. Also, efficient quenching of QDs in an MB through electron transfer still need to be improved. There are two ways to efficient quantum dot quenching through electron transfer— (1) optimize the quencher-QD ratio, and (2) minimize the quencher-QD distance upon the formation of DNA hairpin structure. We will leverage the two approaches using C_{60} to improve the performance of DNA sensing.

2. Experimental

2.1 Chemical and Material.

Iron(II) chloride tetrahydrate, iron(III) chloride hexahydrate, trichloro(1H,1H,2H,2H-perfluorooctyl)silane, hexadecyltrimethylammoniumbromide (CTAB), tris(2-carboxyethyl)phosphine hydrochloride, n-[3-(Trimethoxysilyl)propyl]ethylenediamine, hexamethylenediamine, n-(2-Aminoethyl)maleimide trifluoroacetate salt, n-(2-Aminoethyl)-3-aminopropyltrimethoxysilane (AEAPTMS), tris(2-carboxyethyl)phosphine (TCEP), 6-mercapto-1-hexanol (MCH), and 20X saline-sodium citrate (SSC) buffer were purchased from Sigma-Aldrich. 10X phosphate buffered saline (PBS) buffer was obtained from GIBCO. Malonic acid C60 were purchased from Solaris Chem Inc.

QDs (540,588,610nm emission wavelengths) with thick layer shell were purchased from Ocean NanoTech. The QDs were coating with an ~4-nm thick amphiphilic polymer. The thickness of total layers is about 4nm. QDs (540, 575 nm emission wavelengths) with thin layer shell were obtained from Cytodiagnostics. The thickness of shell layer is less than 1 nm.

All DNAs used in experiments were obtained from LGC Biosearch Technologies. The MB contains 32-bases single-stranded DNA with a 5’ and 3’ ends modified by thiol and amine groups, respectively. The sequence of the MB DNA probe is 3’ GCGCGTCAACATCAGTCTGATAAGCTACGCGC 5’. The sequence of target DNA is 3’ TAGCTTATCAGACTGATGTTGA 5’.

2.2 Experiment

2.2.1 Magnetic particle synthesis

The magnetic nanoparticles were synthesized based on the previous method [28]. In 500 ml flask, 790 mg $FeCl_2$ and 2162 mg $FeCl_3$ were dissolved in 110 mL DI water and heated up to 60^{o}C with stirring. The addition of 40 mL (25 wt%) ammonium hydroxide turned the color of liquid from yellow to black. The solution mixture was heated up to 90^{o}C to dissolve 5 mg CTAB for 30 min and then quenched to room temperature. The magnetic nanoparticles were then rinsed using purified with DI water.

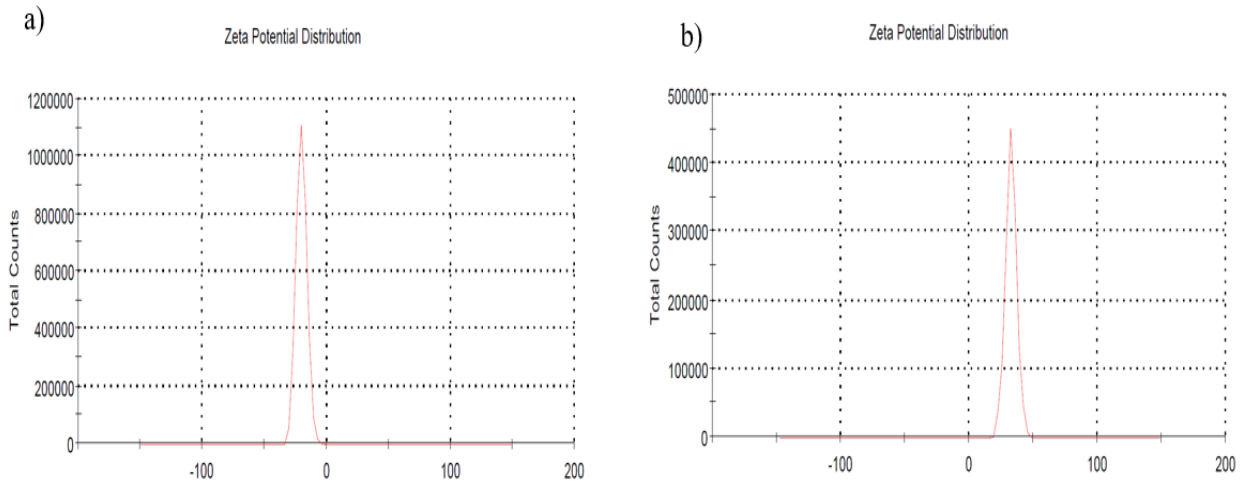

Figure 2.1 Functionalization of amine groups on magnetic nanoparticles turns their surfaces into positive charged. Zeta potential before a) and after b) AEAPTMS coating.

The 100 mg magnetic nanoparticles obtained in the previous step were dispersed into a 150 mL ethanol/water solvent mixture. Three milliliters AEAPTMS and ammonium hydroxide were added dropp-wise into the mixture followed by a 24 hours sonication. The final product was separated

from the solution and washed with DI water, acetone and ethanol. The precipitated amine coated magnetic nanoparticles were dried at room temperature under vacuum. The surface changed from carboxyl to amine, which can be proved through zeta potential measurement (Fig. 2.1）

2.2.2 Conjunction of magnetic nanoparticle-quantum dots- MB-C_{60} (QD-C_{60}MB@MNP)

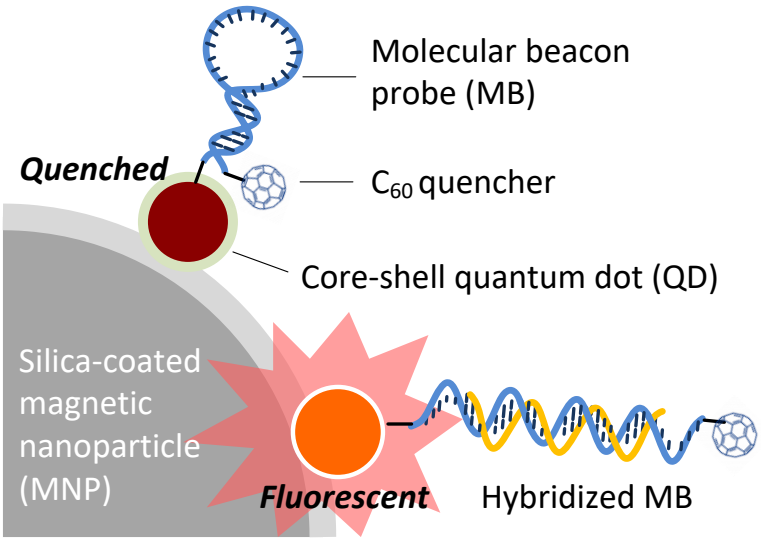

Figure 2.2 Schematic of QD-C_{60} MB@MNP and hairpin DNA hybridization process.

The magnetic nanoparticle linked carboxyl-functioned QDs (610 nm emission wavelength) through a typical conjugation method based on 1-ethyl-3-(3-dimethylaminopropyl) carbodiimide (EDC) and n-hydroxysuccinimide (NHS) mediated cross-coupling. 0.01 nM Carboxylated QDs, 2 mM EDC and 5 mM NHS in 100 mM MES was incubated for 15 min, mixed with a 20 μl amine magnetic nanoparticle solution, and incubated for 1 hour. By introducing 15 μl 100M 2-maleimidoethylamine, the NHS-functionalized QDs on MNP were converted to maleimide for the linkage of oligonucleotide molecular probe through a thiolated 3’-terminal. The 5’-terminal amino

group of the oligonucleotide enabled the conjugation of carboxylated fullerene using EDC/NHS coupling reagents. The MBs particles were rinsed with methanol and redispersed in 1X PBS buffer and annealed at 80^0C before assay. The final schematic of the nano-sensor and DNA detection are summarized in Fig. 2.2.

2.2.3 Conjunction of C_{60}-quantum dots on glass.

The assembly of QDs on a glass surface requires four steps: 1) glass surface salinization, 2) QDs coupling, 3) linker coupling and 4) C_{60} conjugation. In brief, the cover glasses were cleaned by piranha solution for 15 min and then rinsed with DI water. Then the nitrogen gas dried cover glasses were immersed in an amino-silane solution (methanol 10 ml, acetic acid 500 ul, AEAPTMS 100 ul) for 30 min. The amine-modified cover glass was then treated with a mixture of carboxylated QDs, EDC, and NHS for an hour to immobilize a monolayer of QDs. The sample was further treated with hexamethylenediamine in 1X PBS buffer for one hour to produce amine groups on the immobilized QDs. In the final step, carboxylated C_{60} was immobilized on the amine-functionalized QDs through EDC, and NHS, followed by a 1-hour incubation.

2.2.4 Microchip-farbrication

Fluorescence measurement of QD-C_{60}MB@MNP probes and the DNA detection assays were performed in microchips. The device configuration has a well-defined chamber height that ensures a consistent optical path for fair measurements.

2.2.4.1 Fabrication of the microchip for drop detection

As shown in Fig. 2.3, the fabrication started with the hydrophilic treatment of glass by evaporation reaction of trichloro(1H,1H,2H,2H-perfluorooctyl)silane at 90^{o}C for an hour. Hydrophilic patterns were produced the hydrophobic glass surface by performing oxygen plasma treatment in Plasma Etch (Carson City, NV, USA) through a hole-patterned mask. After mask removal, the aqua solution will tend to stay in the hydrophilic hole patterns. A 1-mm thick glass with 1.5 cm × 0.7 cm rectangle opening served as a spacer to sustain liquid pillars with a consistent dimension at the designated hydrophilic areas in the chamber. After loading the analyte, the chip was enclosed by a thin glass secured by two pieces of magnet. By pressing the cover glass, the liquid drop will contact the top glass to form a liquid pillar. The light path went through the center of the liquid pillar during measurement leaving a negligible influence of optical fringe on the observation.

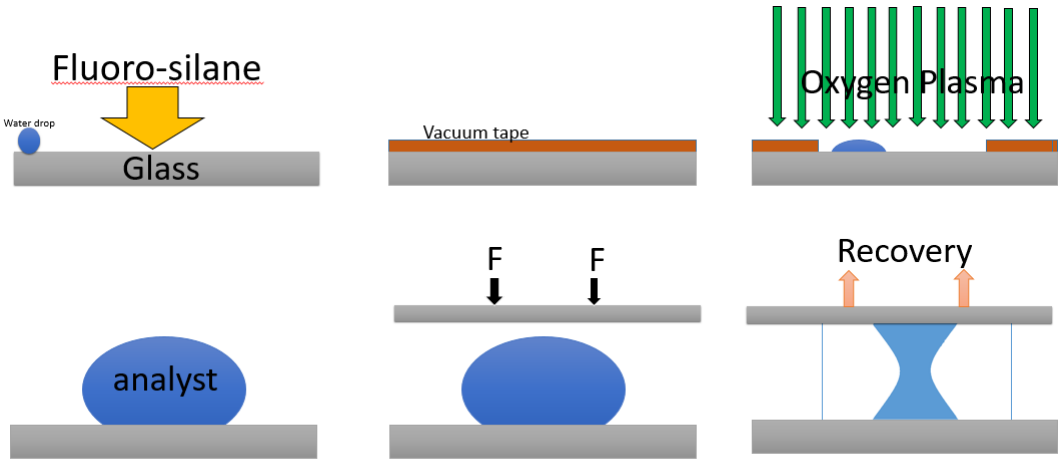

Figure 2.3 Microchip for aqua detection with a water drop located on the hydrophilic area of the glass surface.

2.2.4.2 Fabrication of the microchip for magnetic concentration.

To facilitate an assay with magnetic concentration, we designed a microchip using a thin PDMS spacer to form a connected circular chambers that contain a 3-mm diameter reservoir for liquid loading connected and a 1.5-mm diameter hole for analyte detection. The fluidic chamber is enclosed by two PEG-treated glass slides fabricated by the following process. The glass slides were first treated to create amine groups using AEAPTMS. A mixture of 70-μl PEG solution prepared by dissolving 8-mg PEG solute in 0.1M sodium bicarbonate was used to functionalize the amine treated glass slides. The treatment was carried out in dark and high humidity overnight. After rinsed in DI water and N_2 dried, the treated samples were stored in the dark at -20^0C before usage. To perform detection, we dropped a 5-μl mixture of analyte and MB solution in the 3-mm circular reservoir, enclosed the chamber with a PEG-treated glass, and tapped the microchip to transfer the solution to the 1.5-mm reservoir. The solution volume was large enough to fill the entire 1.5-mm reservoir and the tapping method allowed us to transfer and confine the liquid in the small reservoir for detection without generating bubbles or leakage. As shown in Fig. 2.5 (a) and (b), the complete filling of the liquid in the chamber eliminated the background noise created by the light scattered from the edge of the liquid-air interface. When applying a magnetic needle on the top of the chamber, the magnetic particle-coupled QDs can be attracted and concentrated on one spot.

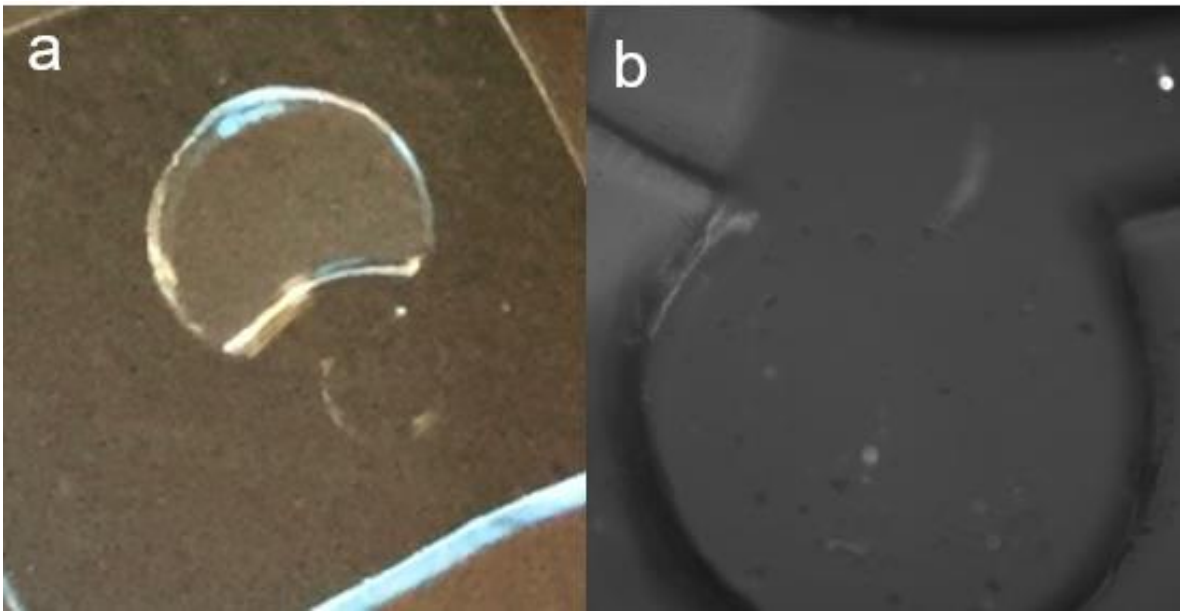

Figure 2.4 (a) Image of the microchip with the 1.5-mm reservoir filled with the analyte solution. (b) Analyte solution in the microchip under 10X magnification.

2.2.4.3 Flow cell for analytes in magnetically concentrated condition

At last, we also developed a flow cell for capture magnetic QDs by applying magnetic blade. The first, we made a flow channel mode by cutting 0.8 mm wide vacuum tape on glass, then assembled two 140 um thin glass on mode to made an even height. The third step was treating the glass mode with Trichloro(1H,1H,2H,2H-perfluorooctyl)silane. After the treatment, we fixed a blade on the top of the thin glass and spanning the vacuum tape pattern. In the last step, we poured PDMS solution with a ratio of 15:1 to curing agent. The magnets were attached to the blade to form a magnetic blade. The fabrication process shows in Fig. 2.5 a. Fig. 2.5 b shows the flow cell can capture the QD@MNP. The result shows the high ability to capture QD@MNP, but since it costs time to load analyte into the flow cell, we prefer to use Microchip introduced in chapter 2.2.4.2.

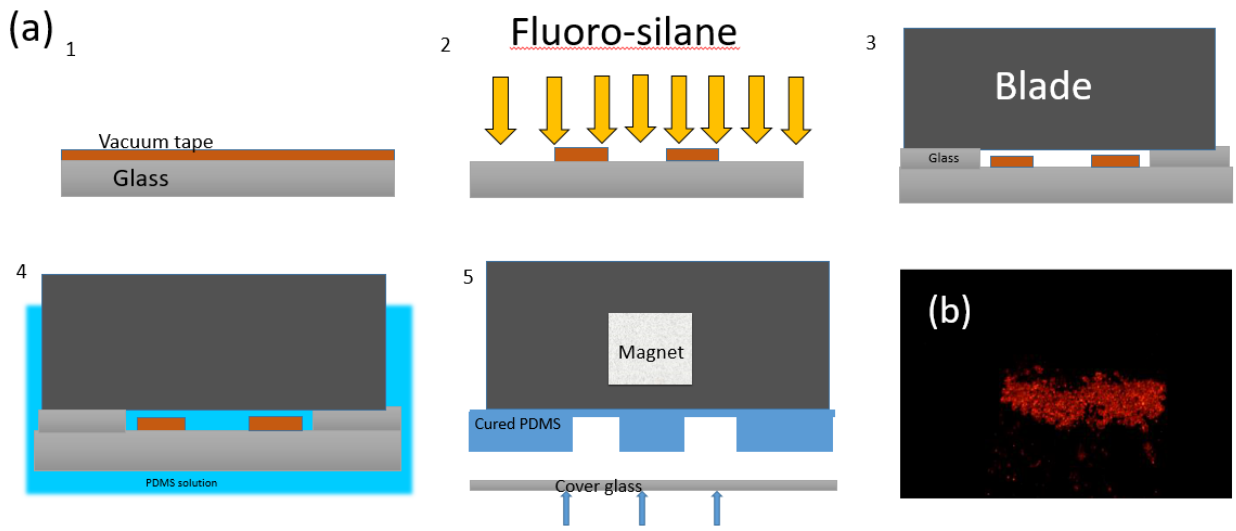

Figure 2.5 (a) Schematic of fabrication flow cell for magnetic nanoparticle capture. (b) QD@MNP are captured by a magnetic blade in the flow cell.

2.2.4 Characterization setup

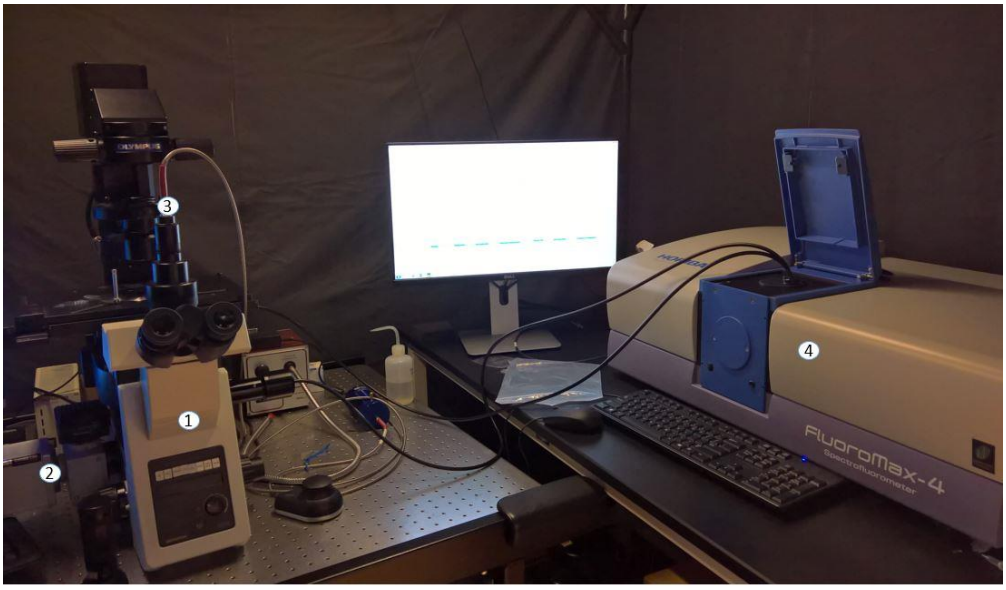

Figure 2.6 The instruments for DNA optical detection. ○1 is the microscope. ○2 is the monochromatic and color CCD camera.○3 is the fiber-coupled spectrometer (Ocean Optics HR4000). ○4 is FuloroMax-4 spectrometer connecting with a microscope.

The fluorescence images and spectra were analyzed under an inverted fluorescence microscope using an sCMOS camera and a fiber-coupled spectrometer (Ocean Optics HR4000). The QDs quenching experiments were analyzed using a fluorescence microscope integrated with a fiber-coupled spectrofluorometer (Fluoromax-4) as shown in Fig. 2.6.

3. Result and Discussion

3.1 C_{60} quenching to quantum dots.

Photoluminescence measurement in Fig. 3.1 indicates that about 70% of quenching efficiency was obtained in covalently incorporated QD-C_{60} complexes. The QDs used have a 4 nm-thick polymer coating to maintain stable emission. An even more effective quenching is expected to observe in uncoated QDs.

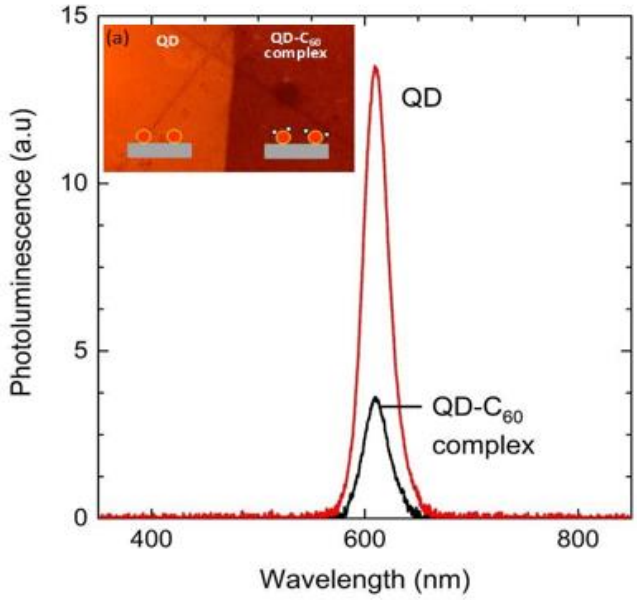

Figure 3.1 Efficient quenching of QD fluorescence by C_{60} evidenced in photoluminescence spectra of QD and QD-C_{60} complex immobilized on a glass substrate under UV excitation (380-395nm excitation wavelength using DAPI 50LP filter). Inset: fluorescent microscopic images of QD and QD-C_{60} complex on a glass surface.

The quenching of QDs depends on the number of C_{60} attached to each of them. Since the C_{60}-to-QD ratio cannot be precisely measured, the ratio was estimated by their proportions prepared for conjugation reaction (Fig. 3.2 a). The C_{60}-to-QD ratio was found to impact the quenching of

different types of QDs with different extents. Fig. 3.2 shows that overall the quenching efficiency increases significantly in a low C_{60}-to-QD ratio, and increases gradually at the large C_{60}-to-QD regime. The quenching efficiency is 20% higher in the QDs with a < 2 nm thick organic coating (540N and 570N) indicating that the electron-transfer-based quenching is highly dependent on the QD-C_{60} distance. The QDs with a 4-nm thick polymer layer (540O, 588O, and 615O) shows gradual changes in quenching efficiency as opposed to a sharp change for the QDs with thin layer coating. QDs with larger band gap (shorter emission wavelength) exhibit relative better quenching efficiency. In the experiment, we found the slight blueshift of PL spectra in higher C_{60}-to-QD ratio. The result may be caused by the oxidation of QDs during long irradiation time [29].

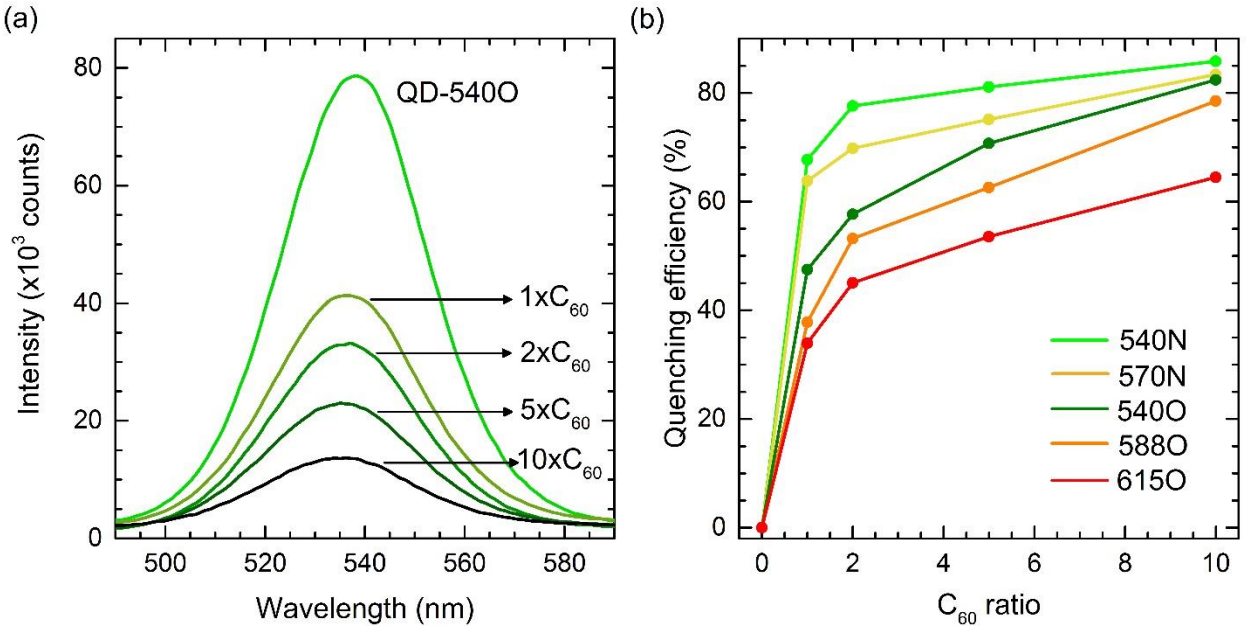

Figure 3.2 The quenching efficiency for different quantum dots. 540N and 570N are the thin layer quantum dots with 540nm and 570nm emission. 540O, 580O, 615O is the thick layer. The measurement was under a LED light source excitation and filtered by DAPI-50LP, and Fluoromax-4 spectrum.

The 4 nm-thick polymer coating on QDs maintains a stable photoluminesce emission. The thick amphiphilic polymer coating prevents the oxidization of QDs. Fig. 3.3 shows the dynamic change

in luminance intensity for polymer-coated QDs and uncoated QDs. Polymer coated QDs maintains stable emission intensity while the PL of those without polymer coating has a decay time of about 100s.

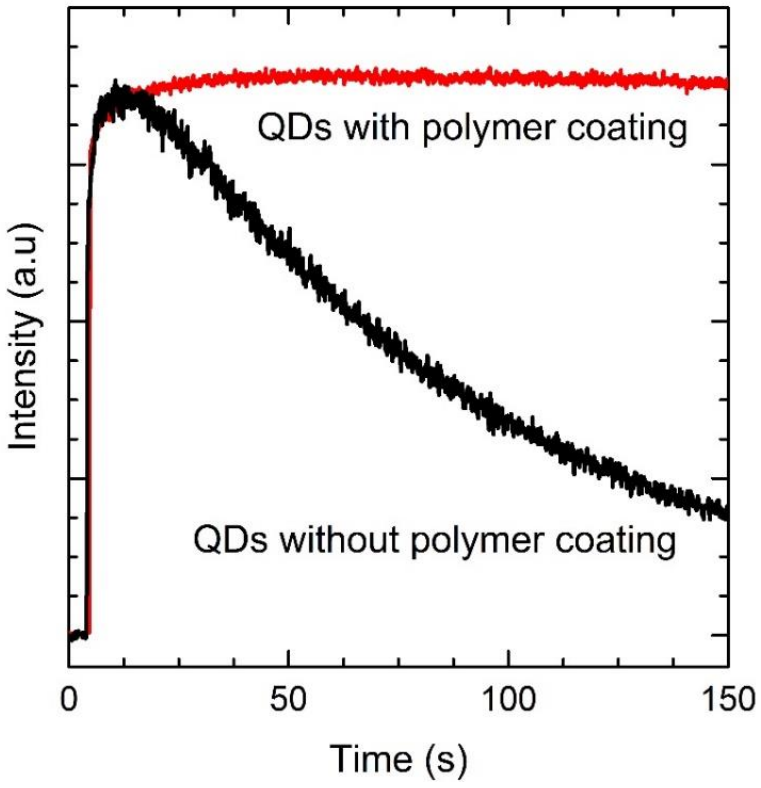

Figure 3.3 Dynamic difference between polymer-coated QDs and QDs

3.2 Magnetic concentration for optical signal enhancement.

Magnetic concentration was demonstrated to significantly boost the detectable quantum dot emission signals. The strategy has two advantages. First, the magnetic particles dispersed in the microchannel for efficient capture of target molecules by reducing the diffusion time. Second, after capturing target molecules, the magnetic particles can be concentrated into a small area to obtain amplified PL signals as the detected signal intensity directly depends on the density of QDs in a

detection area (Fig. 3.4). The glass surface was PEGylated to allow re-dispersion of the concentrated QD@MNP through sonication. The strong emission can be collected by focusing on the concentration plane. We have observed a 10-time increase in the signal detected by a monochromic CCD camera and more than a 5-time increase in the spectrum peak. QD@MNP concentration in chip relate to the intensity enhancement after QD@MNP concentrated. A comparable higher concentration QD@MNP in the microchip results in a thicker layer after magnetic concentrated. The overlay QD@MNP blocks part of the emission from overlapped QD@MNP and leading a less signal enhancement. A result of different magnetic nanoparticles intensity change after magnetic field shows in Fig. 3.5.

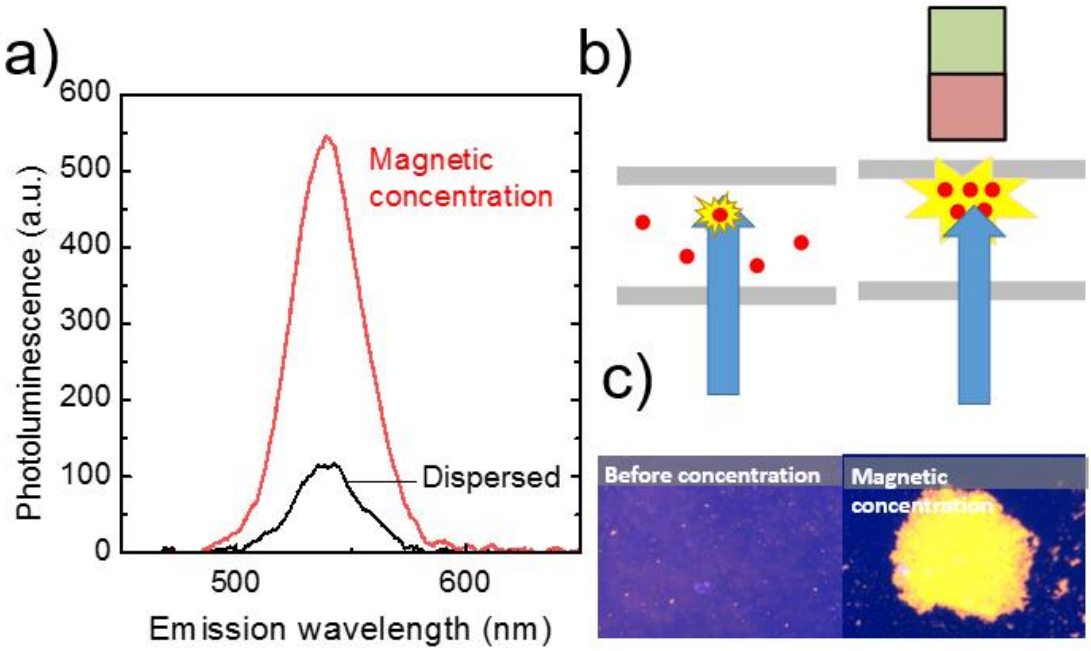

Figure 3.4 (a) PL spectra of the QD@MNP complexes before and after magnetic concentration. The five-time increase in PL signal was observed after magnetic concentration. (b) Schematic of magnetic concentration for signal enhancement. (c) Microscopic images of the QD@MNP complexes before and after magnetic concentration. The measurement shows a 10-time increase in intensity measurement using an SCMOS camera under 380 nm excitation.

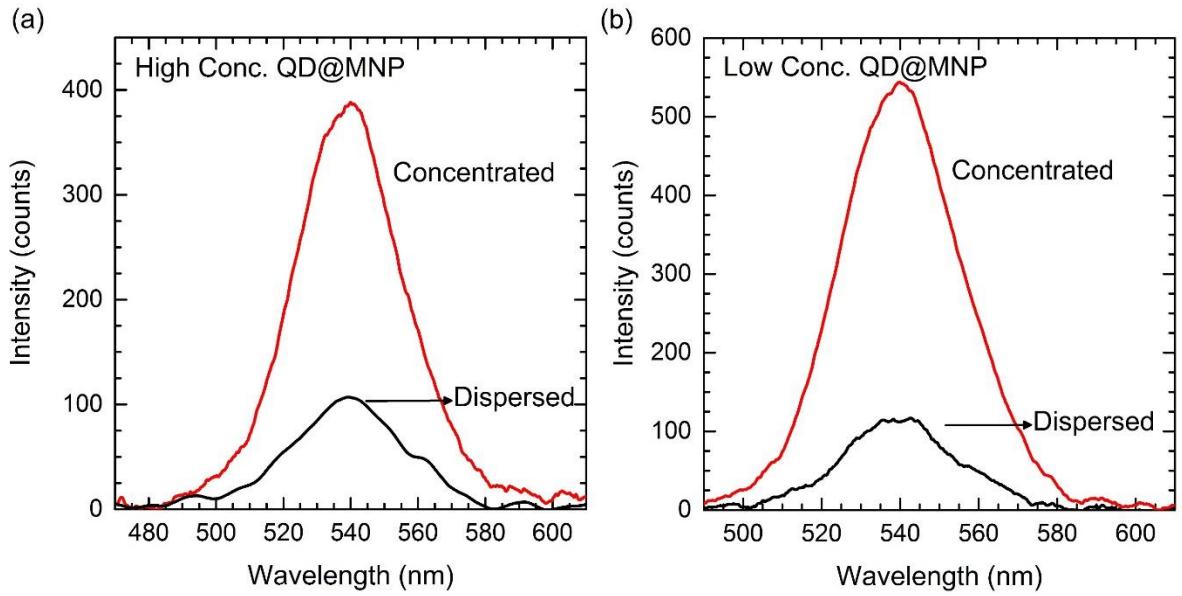

Figure 3.5 Effect of initial concentration of QD@MNP complexes on the signal enhancement after magnetic concentration. PL spectra of dispersed and concentrated QD@MNP with the initial concentration of (a) 0.29 mg/mL QD@MNP and (b) 0.14 mg/mL QD@MNP. The measurement was performed under LED excitation filtered by FX02 excitation.

3.3 DNA detection by QD-C_{60}MB@MNP

3.3.1 DNA detection based on QD-C_{60}MB@MNP

The DNA detection assay started with adding 5 µl analyte samples of various target DNA concentrations ranging from 10 fM to 1 µM separately to 10 µl QD-C_{60} MBs@MNP solutions for 25-minute hybridization. The mixture was then loaded into a 500 µm-thick flow cell described in the previous section for fluorescence analysis. The DNA sensing result is summarized in Fig. 3.6. QD-C_{60} MBs@MNP nano-sensor shows a reasonably broad detection dynamic range. The limit of the detectable signal was observed at 100 fM target concentration.

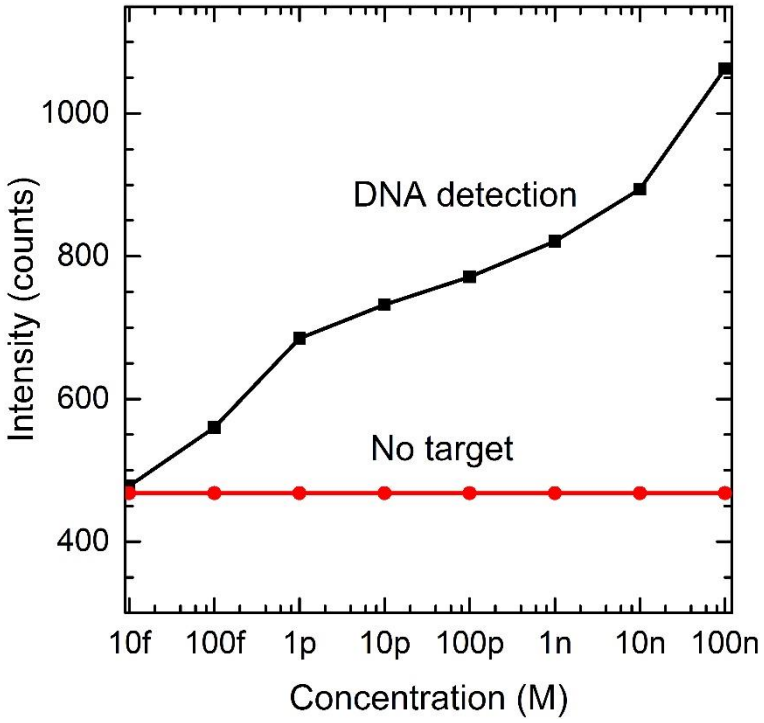

.

Figure 3.6. DNA detection based on QD-C_{60} MB@MNP dispersed in liquid. QDs were excited under 380 nm excitation with a DAPI-50LP filter and measured by an SCMOS camera. orange dashed line indicates the intensity of MBs before hybridization.

3.3.2 Optimization of the time for detecting quantum dots fluorescence signals

Time evolution of PL intensity in Fig. 3.7 shows that the QD-C_{60} based MBs exhibit a stable PL emission over a relatively long excitation duration suitable for the biosensing application. In this experiment, DNA analyte ranging from 10 fM to 100 nM was detected using QD-C_{60}MB@MNP probes. We found that the QDs emission increases with time and stabilizes after about 20 s (Fig. 3.7). So to perform a repeatable DNA assay, the detection signals were all obtained after 20-second excitation.

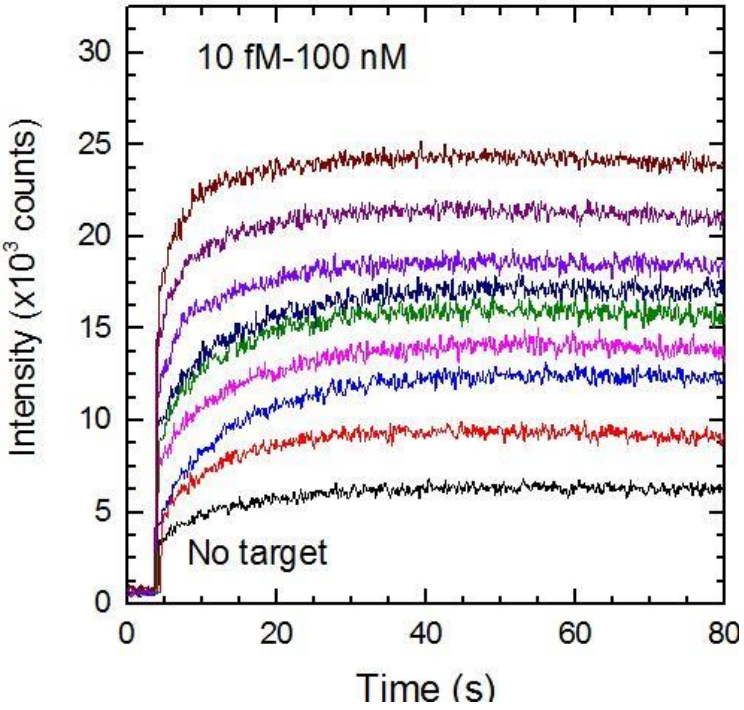

Figure 3.7 Time evolution of the PL signals of QD-C_{60} MB@MNP after DNA hybridization. The measurement was performed using 380 nm excitation with an optical filter TXRED and analyzed by Fluormax-4 spectrofluorometer.

3.3.3 Optimization of DNA probe density on quantum dots for DNA sensing

The density of MB probes immobilized on each QD (or the MB-to-QD ratio) determines the final quencher-to-QD ratio and, therefore, affects the detection limit. A high density of hairpin DNA probes on QDs would reduce the hybridization efficiency due to steric effect, while a low probe density will decrease the number of captures. In our experiment, we immobilized short molecules, 6-mercapto-1-hexanol (MCH), with the MB probes to control the final density of MB probes on QDs. MCH molecules also serve as spacers to support the MB probes sticking out of the surfaces of QDs and prevent nonspecific binding of probes and target molecules. We compared the DNA detection signal under various molar ratios of MCH to MB probe as shown in Fig. 3.8a.

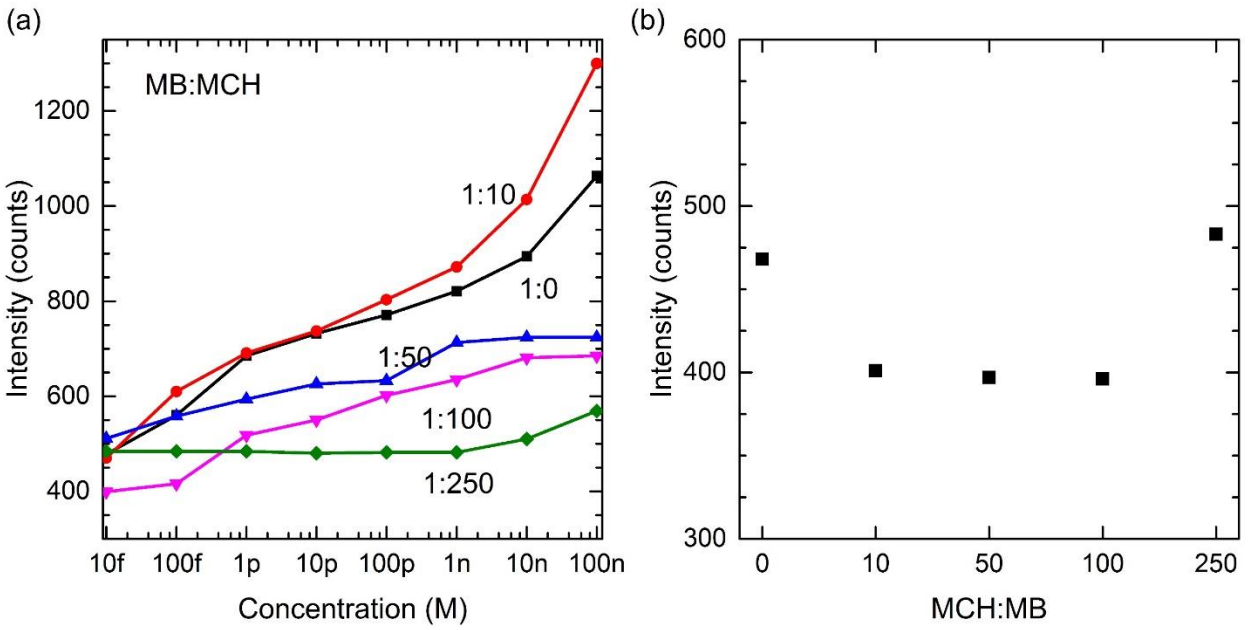

Figure 3.8 QD-C_{60} MB@MNP with different MCH to MB ratio on quantum dots. A) Shows the different MCH to MB ratio on QDs for target DNA detection from 10fM to 100nM. B) Shows the background of different MCH to MB on QD MBs. The measurement was taken under LED excitation filtered by DAPI50LP and CCD camera.

.

The best DNA detection sensitivity was found in the use of a 1:10 MB-to-MCH ratio. Without MCH, the steric interaction among high-density probes may prevent proper formation of MBs upon the annealing process and decrease hybridization efficiency. High background intensity shown in Fig. 3.8(b) may be attributed to a low percentage of properly formed hairpin structures due to the steric effect. As a result, not all the QDs were quenched after annealing. When the MB-to-MCH ratio exceeds 1:50, the sensitivity of DNA detection reduces as shown in Fig. 3.8(a). The low detection sensitivity can be explained by the low DNA probes available for hybridization. There was almost no detectable signal observable with a 1:250 of MB-to-MCH ratio. The number of DNA probe are rarely distributed on QDs in 1:250 of MB-to-MCH ratio, which is proportional to amounts ratio of C_{60} to QDs. As shown in Fig. 3.8(b), the QDs are less quenched and shows higher background intensity before hybridization.

3.3.4 Effect of magnetic concentration on QD-C_{60}MB@MNP-based DNA sensing.

As discussed in chapter 3.2, the QD emission signal can be increased at least 5 times after magnetic concentration under a microscope. Here we compared the QD-C_{60}MB@MNP-based DNA detection on a microchip with and without magnetic concentration (Fig. 3.9). The limit of detection (LOD) was measured to be about 100 pM without magnetic concentration. After magnetic concentration, the LOD decreases to 100 fM. The slope of the curve changes slightly after magnetic concentration due to the high efficiency of the light collection at the focal plane.

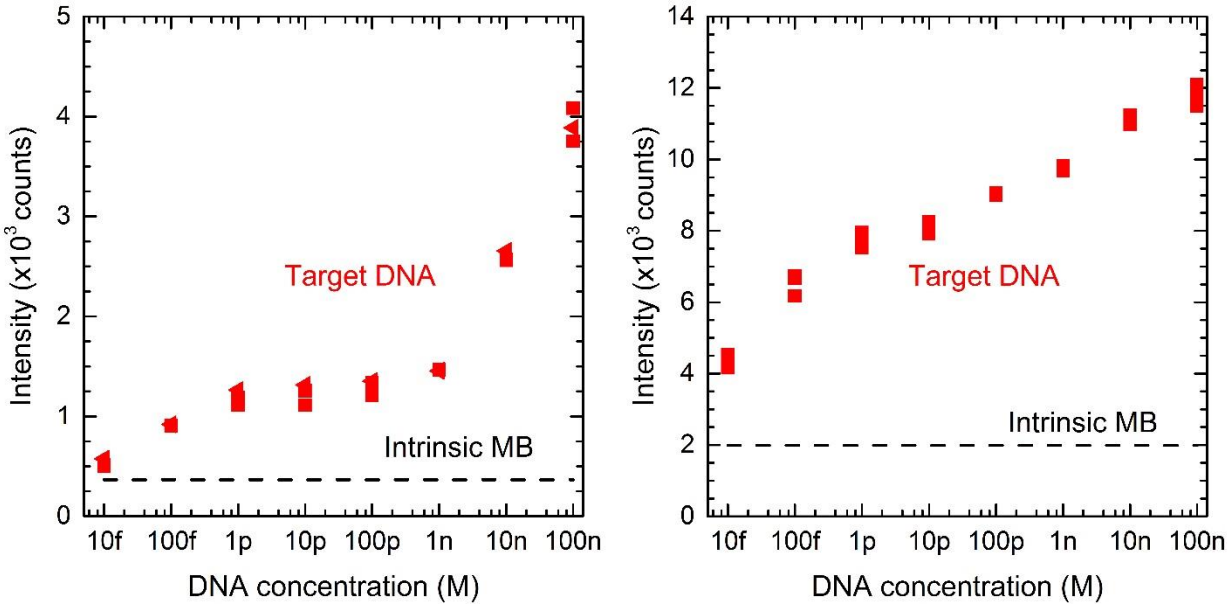

Figure 3.9 QD-C_{60} MB@MNP DNA detection without and with magnetic concentrated. MB fluoresce intensity before assay indicated by the orange dash line. The QDs were excited under LED excitation filtered by TEXRED.

4. Conclusion and Future Work

We have investigated an efficient quenching of QDs using C_{60}. The quenching process is primarily caused by both of electron transfer and FRET, which is sensitive to the C_{60}-QD distance. The distance dependent quenching efficiency also reflects the different quenching behavior of the QDs with different thickness of polymer coating. We have successfully demonstrated the QD-C_{60} based molecular beacon (MB) carried by magnetic particles (QD-C_{60} MBs@MNP) to achieve highly sensitive DNA detection. With the assistance of magnetic concentration, the detection signal was amplified to 5-10 times resulting in a low detection limit of 100 fM. The effect of quencher-QD ratio and MB-MCH ratio on DNA detection were investigated in details. The sensitive detection will find applications in the analysis of low-concertation target, e.g., circulating miRNA for cancer diagnostics or pathogen DNA or RNA for point-of-care detection.

Although QDs have high stability on emission compared with another fluorophore molecular, we still observed fluorescence decay during a continuous excitation. The effect resulting from the generation of oxygen radicals during high-energy excitation in aqueous solutions leads to oxidative decay of QDs. This phenomenon is more observable in the thin layer-coated QDs. The addition of oxygen scavenger or antioxidant chemicals may solve this problem although the extra chemical in analyte solution gives an unpredictable result for detection in vivo or living cells. In future work, we will extend the current experiences to develop multi-target DNA detection coded by multiple QD emission wavelengths. We will also develop a smartphone enabled nucleic acid detection platform that incorporates the smartphone CMOS camera and the developed microchip interface to realize a biosensor technology for point-of-care diagnostics.

5. Reference

1. Jensen, Anton W., Stephen R. Wilson, and David I. Schuster. "Biological applications of fullerenes." *Bioorganic & medicinal chemistry* 4.6 (1996): 767-779.
2. Xu, Zhihua, and Mircea Cotlet. "Quantum Dot–Bridge–Fullerene Heterodimers with Controlled Photoinduced Electron Transfer." *Angewandte Chemie International Edition* 50.27 (2011): 6079-6083.
3. Liu, Dongfang, et al. "Chemical conjugation of fullerene C_{60} to CdSe nanocrystals via dithiocarbamate ligands." *The Journal of Physical Chemistry C* 111.48 (2007): 17713-17719.
4. Stewart, Michael H., et al. "Competition between Förster Resonance Energy Transfer and Electron Transfer in Stoichiometrically Assembled Semiconductor Quantum Dot–Fullerene Conjugates." *ACS nano* 7.10 (2013): 9489-9505.
5. Mullikin, James C., and Amanda A. McMurray. "Sequencing the genome, fast." *Science*283.5409 (1999): 1867-1868.
6. Lia J, Xu C, Zhang Z, Wang Y, Peng H, Lu Z, et al. A DNA-detection platform with integrated photodiodes on a silicon chip. Sens Actuators B Chem 2005;106:378–82.
7. Kjällman, Tanja HM, et al. "Effect of probe density and hybridization temperature on the response of an electrochemical hairpin-DNA sensor." *Analytical chemistry* 80.24 (2008): 9460-9466.
8. Misono, Tomoko S., and Penmetcha KR Kumar. "Selection of RNA aptamers against human influenza virus hemagglutinin using surface plasmon resonance." *Analytical Biochemistry* 342.2 (2005): 312-317.
9. Gui, Zhen, et al. "Direct detection of circulating free DNA extracted from serum samples of breast cancer using locked nucleic acid molecular beacon." *Talanta* 154 (2016): 520-525.
10. Petryayeva, Eleonora, W. Russ Algar, and Igor L. Medintz. "Quantum dots in bioanalysis: a review of applications across various platforms for fluorescence spectroscopy and imaging."*Applied spectroscopy* 67.3 (2013): 215-252.
11. Cady, Nathaniel C., Aaron D. Strickland, and Carl A. Batt. "Optimized linkage and quenching strategies for quantum dot molecular beacons." *Molecular and cellular probes* 21.2 (2007): 116-124.
12. Gueroui, Zoher, and Albert Libchaber. "Single-molecule measurements of gold-quenched quantum dots." *Physical review letters* 93.16 (2004): 166108.
13. Yeh, Hsiao-Yun, et al. "Molecular beacon–quantum dot–Au nanoparticle hybrid nanoprobes for visualizing virus replication in living cells." *Chemical Communications* 46.22 (2010): 3914-3916.
14. Song, Nianhui, et al. "Poisson-distributed electron-transfer dynamics from single quantum dots to C_{60} molecules." *ACS nano* 5.1 (2010): 613-621.
15. Virkki, Kirsi, et al. "Photoinduced Electron Transfer in CdSe/ZnS Quantum Dot–Fullerene Hybrids." *The Journal of Physical Chemistry C* 119.31 (2015): 17561-17572.
16. Xu, Zhihua, and Mircea Cotlet. "Quantum Dot–Bridge–Fullerene Heterodimers with Controlled Photoinduced Electron Transfer." *Angewandte Chemie International Edition* 50.27 (2011): 6079-6083.

17. Bakalova, Rumiana, et al. "Quantum dot-conjugated hybridization probes for preliminary screening of siRNA sequences." *Journal of the American Chemical Society* 127.32 (2005): 11328-11335.
18. Zhang, Chun-Yang, et al. "Single-quantum-dot-based DNA nanosensor." *Nature Materials* 4.11 (2005): 826-831.
19. Riccelli, P. V., et al. "Hybridization of single-stranded DNA targets to immobilized complementary DNA probes: comparison of hairpin versus linear capture probes." *Nucleic acids research* 29.4 (2001): 996-1004.
20. Song, Shiping, et al. "Gold-Nanoparticle-Based Multicolor Nanobeacons for Sequence-Specific DNA Analysis." *Angewandte Chemie International Edition* 48.46 (2009): 8670-8674.4
21. Ertas, Nusret, and Hayriye Eda Satana Kara. "L-Cysteine capped Mn-doped ZnS quantum dots as a room temperature phosphorescence sensor for in-vitro binding assay of idarubicin and DNA." *Biosensors and Bioelectronics* 70 (2015): 345-350.
22. Raichlin, Sara, et al. "Electron-transfer quenching of nucleic acid-functionalized CdSe/ZnS quantum dots by doxorubicin: a versatile system for the optical detection of DNA, aptamer–substrate complexes and telomerase activity." *Biosensors and Bioelectronics* 26.12 (2011): 4681-4689.
23. Cui, Daxiang, et al. "Self-assembly of quantum dots and carbon nanotubes for ultrasensitive DNA and antigen detection." *Analytical Chemistry* 80.21 (2008): 7996-8001.
24. Morales-Narváez, Eden, and Arben Merkoçi. "Graphene oxide as an optical biosensing platform." *Advanced Materials* 24.25 (2012): 3298-3308.
25. Yang, Ronghua, et al. "Noncovalent assembly of carbon nanotubes and single-stranded DNA: an effective sensing platform for probing biomolecular interactions." *Analytical chemistry* 80.19 (2008): 7408-7413.
26. Dong, Haifeng, et al. "Fluorescence resonance energy transfer between quantum dots and graphene oxide for sensing biomolecules." *Analytical Chemistry* 82.13 (2010): 5511-5517.
27. Li, Hailong, et al. "Nano-C_{60}: A Novel, Effective, Fluorescent Sensing Platform for Biomolecular Detection." *Small* 7.11 (2011): 1562-1568.
28. Tourinho, Francisco Augusto, Raymonde Franck, and René Massart. "Aqueous ferrofluids based on manganese and cobalt ferrites." Journal of Materials Science 25.7 (1990): 3249-3254
29. Xu, X. & Li, X. "Enhanced emission of charged-exciton polaritons from colloidal quantum dots on a SiN/SiO_2 slab waveguide." *Sci, Rep.* 5 (2015).